Biomaterials Science

Thermoplastic zwitterionic elastomer with critical antifouling properties

Journal:	*Biomaterials Science*
Manuscript ID	BM-ART-02-2022-000190.R1
Article Type:	Paper
Date Submitted by the Author:	27-Mar-2022
Complete List of Authors:	Wang, Kun; University of Illinois at Chicago, Arado, Theo; University of Chicago Laboratory Schools Huner, Ardith; University of Chicago Laboratory Schools Seol, Hyang; University of Illinois, Chicago Liu, Xuan; University of Illinois at Chicago Wang, Huifeng; University of Illinois at Chicago Hassan, Lena; University of Illinois at Chicago, Chemical Engineering Suresh, Karthika; University of Illinois at Chicago Kim, Sangil; University of Illinois, Chicago, Chemical Engineering Cheng, Gang; University of Illinois at chicago, Chemical Engineering

Thermoplastic zwitterionic elastomer with critical antifouling properties

Kun Wang,[1] Theo Arado,[2] Ardith Huner,[2] Hyang Seol,[1] Xuan Liu,[1] Huifeng Wang,[1] Lena Hassan,[1] Karthika Suresh,[1] Sangil Kim,[1*] and Gang Cheng[1*]

1. Department of Chemical Engineering, University of Illinois Chicago, Chicago, IL 60607, USA
2. University of Chicago Laboratory Schools, Chicago, IL 60637, USA

Kun Wang, Theo Arado, and Ardith Huner contribute equally to this work.

*Corresponding authors: sikim@uic.edu, gancheng@uic.edu

Abstract

Thermoplastic elastomers are widely used in the medical industry for advanced medical and healthcare products, helping millions of patients achieve a better quality of life. Yet, microbial contamination and material-associated biofilm on devices remain a critical challenge because it is challenging for currently available materials to provide critical antifouling properties, thermoplasticity, and elastic properties simultaneously. We developed a highly flexible zwitterionic thermoplastic polyurethane with critical antifouling properties. A series of poly((diethanolamine ethyl acetate)-*co*-poly(tetrahydrofuran)-*co*-(1,6-diisocyanatohexane)) (PCB-PTHFUs) were synthesized. The PCB-PTHFUs exhibit a breaking strain of more than 400%, a high resistance to fibroblast cells for 24 h, and the excellent ability to prevent biofilm formation for up to three weeks. This study lays a foundation for clarifying the structure-function relationships of zwitterionic polymers. This thermoplastic PCB-PTHFU platform, with its unmatched antifouling properties and high elasticity, has potential for implanted medical devices and a broad spectrum of applications that suffer from biofouling, such as material-associated infection.

Keywords

Zwitterionic polyurethane, thermoplastic polyurethane, biofilm, elastic polyurethane, implanted medical devices

1. Introduction

Each year, millions of patients suffer from device-associated infections caused by the colonization of microbes and biofilms on medical devices. Implant-associated infections can lead to device failure, prolonged treatment and hospital stays, and chronic infections, which can be life-threatening.[1] For example, the mortality of catheter-related bloodstream infections reaches 12% - 25%.[2] A biofilm is a complex organic material consisting of clusters of bacterial cells growing within an extracellular polymeric substance produced by bacteria. After implantation, microorganisms may quickly attach to a host protein layer formed along the device surface.[3] Once a biofilm forms, it shows remarkable resistance to removal.[4] Thus, high-dose antibiotics and/or frequent implant replacements are required to prevent biofilm formation. However, implant replacements are costly and ineffective, and the likelihood of re-infection on the new implant is high.[5] The antibiotic agent is depleted from the surface over time. Moreover, antibiotics increase antimicrobial resistance, especially for bacteria with high adaptive resistance, such as *Pseudomonas aeruginosa*.[6, 7] To address the unsatisfactory performance of the current materials used for biomedical applications, there is a critical need to develop new and effective materials with a pronounced resistance to biofilm formation. In particular, the prevention of biofilm formation is likely the most feasible approach for addressing infections associated with implanted medical devices.

Thermoplastic polyurethanes (TPUs) have been widely used as medical implants, sutures, and tissue engineering scaffolds due to their excellent mechanical strength, elasticity, and biocompatibility [8-10]. However, current TPUs lack a critical antifouling property to prevent biofilm formation and subsequent implant-associated infections, especially in complex biological environments and fluids, such as urine and body fluids.[7, 11, 12] Poly(ethylene glycol) (PEG)-based functionalization has been broadly employed to modify polyurethane surfaces and improve antifouling properties.[13-16] However, several studies have demonstrated that PEG-based materials are insufficient to resist blood protein adsorption.[17, 18] Furthermore, it has been observed that PEG can trigger foreign body reactions and immune responses,[19, 20] which hinder biomedical applications of PEG-modified materials as implanted medical devices. In comparison, zwitterionic polymers have demonstrated superior antifouling properties and the potential to address biofouling-related challenges, potentially due to the synergistic benefits of their neutral charge and the hydration shell formed by ionic solvation with water.[18, 21-31]

Several approaches have been extensively studied to incorporate zwitterionic functional groups onto materials.[32] Surface modification methods are commonly used, as this process is simple and time-saving.[33] However, the coating layer can be quickly depleted from the material surface in aqueous media due to the high water solubility of most zwitterionic agents. After detachment of the zwitterionic coating, the underlying substrate loses its antifouling property, which can cause a foreign body reaction *in vivo*. Thus, the surface coating method is not suitable for bio-application. Another approach is to tether zwitterionic polymers on a material surface by the "graft-from" method, which has better stability than surface coating.[34-36] However, this method involves complicated and time-consuming surface modification procedures that hinder technological adoption for high-volume production. Recently, zwitterionic polymers have been developed to incorporate zwitterionic functional groups in bulk material, which can overcome the disadvantages of “graft-to” and “graft-from” methods.[25, 37-40] Nevertheless, due to their high polarity and solubility in water, linear zwitterionic materials usually exhibit a relatively low Young’s modulus and unsatisfactory elasticity. Although crosslinking was applied to increase the mechanical properties of zwitterionic materials [41], the large-scale fabrication and shaping of crosslinked materials are hard. A robust and elastic material is required for many implanted medical devices, for example, endotracheal tubes, peritoneal catheters, urinary catheters, central venous catheters, and various artificial tissues[42-44]. Thus, a zwitterionic elastomer with strong antifouling and elasticity properties is urgently needed to address the issues mentioned above.

Herein, we report a highly elastic zwitterionic thermoplastic polyurethane with critical antifouling properties. We designed and synthesized a series of poly ((diethanolamine ethyl acetate)-*co*-poly(tetrahydrofuran)-*co*-(1,6-diisocyanatohexane)) (PCB-PTHFUs). The PCB-PTHFUs carry different amounts of hydrolyzable diethanolamine ethyl acetate (DEAEA) diol chain extenders and poly(tetrahydrofuran) (PTHF) soft domains in polymeric backbones. The chemical structure, thermal stability and transition behavior, mechanical strength, rheological behavior, surface fibrinogen adsorption, mammalian cell attachment, bacteria attachment, and biofilm formation of the PCB-PTHFUs were studied.

2. Experimental section

2.1 Materials

PTHF with a molecular weight of ~1000 Da (PTHF 1000), PEG with a molecular weight ~300 Da, ethyl acrylate, and phosphate-buffered saline (PBS) were purchased from Sigma–Aldrich (St. Louis, Missouri, USA). 1,6-Diisocyanatohexane (HDI) and extra dry grade of dimethylformamide (DMF) were obtained from Acros Organics (Pittsburgh, Pennsylvania, USA). Diethanolamine, fluorescein isothiocyanate (FITC) isomer and bovine fibrinogen were purchased from Alfa Aesar (Haverhill, Massachusetts, USA). Methanol was obtained from Fisher Scientific (Ottawa, Ontario, Canada). Diethyl ether was purchased from VWR Chemicals (Mississauga, Ontario, Canada). DMAO was purchased from Biotium (Fremont, California, USA). Commercially-available medical-grade polyurethane (API-PU) was obtained from American Polyfilm (Branford, Connecticut, USA).

2.2 Synthesis of DEAEA

The synthesis route of DEAEA was reported in our previous work.[21] In a typical reaction, a one-neck round flask with a magnetic stirrer was covered by aluminum film and placed in a water bath at 35 ℃. Ethyl acrylate (30.3g, 0.299 mmol) was added to a round flask. Diethanolamine (28.6g, 0.272 mmol) at a molar ratio of $N_{Diethanolamine}$: $N_{Ethyl\ acrylate}$ = 1: 1.1 was added to the flask dropwise with stirring. After an overnight reaction, the resulting DEAEA was concentrated in a rotary evaporator (Heidolph, USA) at 50 ℃ for two h. The concentrated DEAEA was further purified by flash chromatography using a dichloromethane and methanol mixture (4:1) as the eluent. The resulting DEAEA was a colorless oil with a 94% yield. The chemical structure of DEAEA was measured by ^{1}H Nuclear magnetic resonance (NMR) (DPX400, Bruker, USA). ^{1}H NMR (400 MHz, $CDCl_3$, ppm): 1.17 (t, 3H), 2.39 (t, 2H), 2.54 (t, 4H), 2.76 (t, 2H), 3.510 (t, 4H), 4.04 (m, 2H).

2.3 Synthesis of PCB-PTHFUs

Five PCB-PTHFUs were synthesized with different molar ratios of DEAEA, PTHF1000, and HDI ((N_{DEAEA} + $N_{PTHF1000}$) : N_{HDI} = 1:1). PCB-PTHFU-0, PCB-PTHFU-25, PCB-PTHFU-50, PCB-PTHFU-75, and PCB-PTHFU-100 were prepared with DEAEA to HDI ratios of 0, 0.25, 0.5, 0.75, and 1, respectively. Before the reaction, PTHF1000 was placed in a vacuum oven at 100 ℃ for two h in advance to remove any moisture in the material. Afterward, the PTHF1000 was transferred to a three-neck round flask equipped with a mechanical stirrer and a nitrogen line. When the flask temperature reached a constant 80 ℃ in an oil bath, HDI was added to the flask dropwise. The mixture reacted at 80 ℃ under stirring at 400 rpm for two h to form a pre-polymer.

Then, after a chain extender, DEAEA was added dropwise, the mixture reacted at 80 ℃ under stirring at 400 rpm for 4 - 24 h depending on DEAEA ratios. DMF was added once the viscosity increased, approximately one h after the addition of DEAEA. The temperature was then lowered to 60 ℃, and methanol was added as a quencher. After the system reacted at 60 ℃ for another 0.5 h, the resulting polymers were precipitated in diethyl ether to remove oligomers and unreacted monomers. The purified polymers were transferred to PTFE dishes and dried in a vacuum oven at 100 ℃ to remove the residual solvent. After drying, flat films could be peeled off from the PTFE dishes. The prepared PCB-PTHFUs were submerged into DI water for two days and then dried to prepare hydrolyzed PCB-PTHFUs. Poly (PEG-*co*-PTHF-*co*-HDI)-50 (PEG-PTHFU-50) was also synthesized by the same method with PEG300, PTHF1000, and HDI (N_{PEG300}: $N_{PTHF1000}$: N_{HDI} = 0.5:0.5:1).

2.4 Gel permeation chromatography (GPC)

The weight average molecular weights (M_w) and polydispersity (PDI) of PCB-PTHFUs were determined by GPC at 70 °C on a Waters 2412 using a series of monodisperse polyethylene oxide as standard and DMSO as the fluent with a flow rate of 1.0 mL/min.

2.5 Fourier transform infrared spectroscopy (FT-IR)

The molecular structures of the PCB-PTHFU and PEG-PTHFU-50 samples were analyzed at room temperature by an FT-IR spectrometer (Nicolet iS50, Thermo Nicolet, USA) in attenuated total reflection (ATR) mode. Each piece was scanned 32 times from 600 to 4000 cm^{-1} at a spectral resolution of 4 cm^{-1}. Measurement of ambient air was set as a reference in prior, and the sample curves were normalized with the peak of air moisture.

2.6 Differential scanning calorimetry (DSC)

DSC (TA Instruments, USA) was performed to determine the phase transition behavior of the PCB-PTHFU samples. 7 mg of sample was loaded into a Tzero aluminum pan. The heating and cooling rates were ten ℃/min, and the experiments were performed with an N_2 flow rate of 50 mL/min. The sample was heated from room temperature to 180 ℃ and then cooled to -90 ℃ to investigate the thermal behavior during cooling. The heating/cooling behavior was analyzed from -90 ℃ to 180 ℃.

2.7 Thermogravimetric analysis (TGA)

TGA (PerkinElmer, USA) was performed to determine the thermal stability of the PCB-PTHFU samples. First, 5 mg of each piece was placed in a standard platinum pan. The temperature was

increased from 50℃ to 800℃ at a rate of 5℃/min in an air atmosphere. The temperature was held at 110℃ for 180 min to remove any moisture.

2.8 Mechanical testing

An EZ-Test Compact Bench Testing Machine (Shimadzu, Japan) was used to characterize the compression and tensile properties of the PCB-PTHFU materials. Both unhydrolyzed PCB-PTHFUs in the dry state and hydrolyzed PCB-PTHFUs that had equilibrated in water for two days (without drying) were studied. PEG-PTHFU-50 was also studied as a reference. Each material was cut to a disk with a diameter of 8 mm and a thickness of 2 mm in a compression test. The disk was then compressed to failure at a 1 mm/min rate with a 5000 N maximum load cell. The Young's modulus was obtained from the linear portion of the compression strain-stress curve. For the tensile test, each material was cut to a dumbbell-shaped specimen with a gauge length of 55 mm and a gauge width of 5 mm. The specimen was stretched to breakage at a 500 mm/min stretching speed.

2.9 Rheological testing

An MCR 302 rheometer (Anton Paar, Austria) equipped with 8-mm parallel plates was used to analyze the rheological properties of the PCB-PTHFUs. Strain sweep measurements were performed from 0.1% to 100% with a frequency of 10 rad s^{-1} to verify the linear viscoelastic regime. A lower temperature ranging from −35 °C to 60 °C and a higher temperature ranging from 60 °C to 150 °C were applied for each material under a strain of 1% and a frequency of 10 rad/s. Frequency sweep tests were conducted at 37 °C under a strain of 1%.

2.10 Protein adsorption

As described in our previous work, a fluorescence method was used to evaluate the protein adsorption on the PCB-PTHFUs.[45] In brief, after the PCB-PTHFU, API-PU, and PEG-PTHFU-50 were cut to 8-mm-diameter, 2-mm-thick discs, the discs were submerged in water or pH-8.5 buffer for varying lengths of time. Afterward, the discs were equilibrated in PBS buffer for 20 min and then transferred to a 24-well flat-bottomed polystyrene plate. Each sample was treated with 1 mL of 1 mg/mL FITC-labeled human fibrinogen (FITC-Fg) solution. The samples were equilibrated in the FITC-Fg solution for 30 min to allow protein adsorption. Subsequently, the samples were lifted by a sterile tweezer and gently rinsed in PBS buffer three times to remove excess dye solution. The samples were then transferred to a glass slide and analyzed by Olympus IX81 fluorescent microscope (Olympus, Japan) with a 20 x objective lens through an FITC filter. Three samples were measured for each material under each hydrolysis condition. The exposure time was fixed at

200 ms for all samples. Ten images at different spots were taken for the surface of each sample. The fluorescence intensity of each image was analyzed by ImageJ software.

2.11 Mammalian cell attachment

PCB-PTHFU, API-PU, and PEG-PTHFU-50 discs were equilibrated in deionized water (DI) for 14 days, sterilized by ultraviolet (UV) radiation for 30 min, and placed in a 24-well tissue-culture coated flat-bottomed polystyrene plate. NIH-3T3 cells were seeded at 10^5 cells/well in a mixed culture containing 89% Dulbecco's Modified Eagle Medium (DMEM) 1640 medium, 10% fetal bovine serum (FBS), and 1% penicillin-streptomycin. The material discs with the cells were maintained in a 37℃ incubator with 5% CO_2 for 24 h to allow cell attachment. Afterward, the samples were transferred to a glass slide by a sterile tweezer. The surface cell coverage was visualized with an Olympus IX81 fluorescent microscope (Olympus, Japan) with a 10x lens. Three samples were measured for each material. Ten images at different spots were taken for the surface of each sample. The surface cell density was calculated by ImageJ software.

2.12 Bacterial attachment

PCB-PTHFU, API-PU, and PEG-PTHFU-50 discs were fully hydrolyzed by equilibrating in DI water for 14 days, dried at room temperature for 24 h, and sterilized by UV radiation for 30 min. The dry sample discs were then soaked in DI water for 30 min. *Pseudomonas aeruginosa* PAO1 was washed and dispersed in sterile PBS buffer at a concentration of 5×10^8 cells per mL n. Next, 1 mL of cell suspension was transferred to each well of a 24-well tissue-culture coated flat-bottomed polystyrene plate. In each well, one sample disc was placed at the bottom. Plates were incubated at 37°C without agitation (static culture) for three h. Afterward, the samples were removed by a sterile tweezer and gently rinsed in DI water three times. The sample surface was treated with DMAO dyes, and then the samples were incubated for 30 min at room temperature. After the staining process, the samples were lifted by a sterile tweezer and gently rinsed in DI water three times to remove excess dye solution. The samples were transferred to a glass slide and analyzed by an Olympus IX81 fluorescent microscope (Olympus, Japan). Ten images at different spots were taken for the surface of each sample. The surface cell density was calculated by ImageJ software. After these measurements, the same samples were soaked in DI water for one hour and then dried at room temperature for 24 h. The samples were evaluated seven times by the same cell attachment method described above.

2.13 Biofilm formation assay

P. aeruginosa PAO1 was washed with sterile PBS and then dispersed in a sterile lysogeny broth medium at a concentration of 10^6 cells/mL. Discs of wet hydrolyzed and dry unhydrolyzed PCB-PTHFU, API-PU, and PEG-PTHFU-50 were sterilized by UV radiation for 30 min and then transferred to a 24-well tissue-culture coated flat-bottomed polystyrene plate with the bacteria suspension. The temperature of the system was maintained at 25 ℃, and half of the media was replaced by fresh Luria-Bertani (LB) media each day. After a varying length of time, one disc of each material was lifted by a sterile tweezer and gently washed with 0.85 wt% NaCl solution to remove loosely bonded cells. Then, the rinsed samples were treated with DMAO dyes and were incubated for 30 min at room temperature. After staining, the samples were lifted by a sterile tweezer and gently rinsed in DI water three times to remove excess dye solution. The samples were then transferred to a glass slide and analyzed by an Olympus IX81 fluorescent microscope (Olympus, Japan). Ten images at different spots were taken for the surface of each sample. The surface biofilm coverage was calculated by ImageJ software.

2.14 Swelling ratio

Discs of each sample were equilibrated in DI water for two weeks. After the discs were taken out of the DI, the surface water was removed entirely by a paper towel (Kimwipes). The discs were weighed and lyophilized, and the dried discs were weighed again. The weight swelling ratio was calculated using the following equation:

$$Q = \frac{M_S - M_D}{M_D}$$

where Q is the swelling ratio, M_S is the mass after swelling, and M_D is the mass after lyophilization.

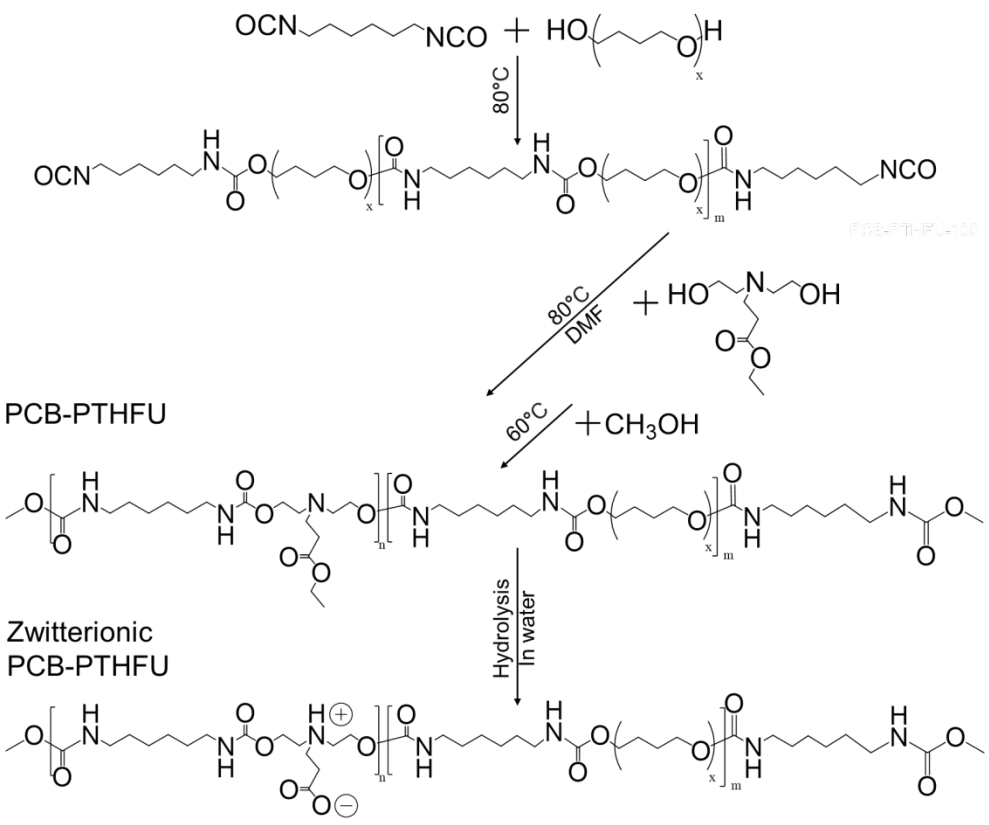

Figure 1. Synthesis route of PCB-PTHFUs.

3. Results and discussion

3.1 Synthesis of PCB-PTHFUs

The structure and molecular weight of the polyol used in polyurethane synthesis significantly affect the mobility and mechanical properties of a polymer. PTHF1000 with an average molecular weight of 1000 Da is favorable for preparing polymers with typical rubber elasticity.[46] To develop a highly elastic zwitterionic thermoplastic polyurethane, we designed and synthesized a thermoplastic polyurethane (TPU) with PTHF1000, DEAEA, and HDI in our study. The PTHF1000 serves as an elastic component that provides the material with high elasticity. DEAEA is a multiple-purpose component that acts as a chain extender and an antifouling precursor. As demonstrated in our previous study, DEAEA undergoes self-catalyzed hydrolysis in the aqueous environment.[21] The hydrolyzed DEAEA segment generates a zwitterionic carboxybetaine (CB) group that can provide critical antifouling properties. DEAEA can be synthesized via a simple Michael addition reaction with a high yield.[21] The high purity of the prepared DEAEA was confirmed by NMR (**Figure S1**). This study designed five different DEAEA/PTHF1000 (PCB-

PTHFU-0, PCB-PTHFU-25, PCB-PTHFU-50, PCB-PTHFU-75) and PCB-PTHFU-100) to tune the mechanical properties of the PCB-PTHFUs and to study their antifouling properties. As a reference, PEG-PTHFU-50 was prepared to compare the behavior of PEG-based material and zwitterionic materials. As shown in **Figure S2**, the number average molecular weight (Mn) is 21, 18, 12, 11, and 3 kDa for PCB-PTHFU-0, PCB-PTHFU-25, PCB-PTHFU-50, PCB-PTHFU-75, and PCB-PTHFU-100, respectively.

3.2 FT-IR spectroscopy

The chemical composition of the PCB-PTHFUs and PEG-PTHFU-50 was characterized by FT-IR analysis (**Figure 2a)**. In the PCB-PTHFUs, the -NCO stretching absorbance at 2250–2270 cm^{-1} is absent, indicating the completion of the reaction and the depletion of all isocyanate groups. Absorption bands for N–H stretching vibrations are observed at 3340 cm^{-1}, and C–H stretching, C=O stretching, C-O-C stretching, and N-H bending are observed at 2920–2860, 1700, 1040–1110, and 1540 cm^{-1}, respectively. The DEAEA to PTHF1000 ratio was adjusted within PCB-PTHFUs. As the DEAEA ratio increased, more C=O, N-H, and C-N bonds occurred in the PCB-PTHFU. Meanwhile, PCB-PTHFUs with higher PTHF1000 contents show higher C-H bond densities. Thus, the integration of the C-H stretches increases with higher PTHF1000 content, with PCB-PTHFU-0 exhibiting the highest level of integration and PCB-PTHFU-100 showing the lowest. At the same time, PCB-PTHFU-0 displays the weakest signal of the N-H stretch, C=O stretch, N-H bend, and C-N stretch, while PCB-PTHFU-100 shows the highest values. The signal change of the N-H stretch, C=O stretch, N-H bend, and C-N stretch is consistent with the ratio of DEAEA and PTHF1000 in PCB-PTHFUs.

3.3 Thermal stability and thermal transition behavior

The thermostability of TPU is an important factor to consider in a material, as it is closely related to the processing and service temperature window. However, the application of TPU can be limited by the relatively low thermal decomposition temperature of urethane bonds.[47] The thermal decomposition temperature is strongly related to the isocyanate and polyol groups used to synthesize TPU. In our study, PCB-PTHFUs were designed with alkyl isocyanate and alkyl polyol, which were found to possess a relatively high degradation temperature among different kinds of TPUs.[48] The thermal stability of PCB-PTHFUs was investigated by TGA, as shown in **Figures 2d** and **2e**. The weight loss at 110 ℃ corresponds to the evaporation of adsorbed water in the samples. Starting from 170 ℃, PCB-PTHFUs follow the typical three-step decomposition process observed

for TPU.[49] In the first stage, mass loss occurs as the urethane bonds decompose and form alcohol and isocyanate groups. Subsequently, the isocyanates dimerize and form carbodiimides. Then, relatively stable N-substituted urea is formed by the reaction between alcohol hydroxyl groups and carbodiimides, which prevents complete volatilization of the resulting chain fragments. In the final stage, the N-substituted urea becomes volatile at higher temperatures, resulting in the loss of the remaining mass. PCB-PTHFU-0, PCB-PTHFU-25, PCB-PTHFU-50, PCB-PTHFU-75, and PCB-PTHFU-100 show an average weight loss of 30.2% between 170 ℃ and 300 ℃ in the first stage, combined with a 69.8% weight loss in the second and third stage from 300 ℃ to 580 ℃. PCB-PTHFU-0 shows the lowest decomposition temperature among the PCB-PTHFUs, presumably due to the absence of DEAEA and thus weaker intermolecular hydrogen bonding. For PCB-PTHFU-25, PCB-PTHFU-50, PCB-PTHFU-75, and PCB-PTHFU-100, the temperature at which weight loss begins increases with the PTHF1000 ratio in the polymer. This trend in degradation temperature change has been previously reported, as TPU with a higher soft segment concentration is more thermally stable and exhibits a higher degradation temperature.[48] Overall, the PCB-PTHFUs show high thermal stability comparable to that of commercially available TPUs,[50], which is advantageous for the fabrication and application of the material.

The thermal transition behavior of PCB-PTHFUs was analyzed by DSC. BEFORE HYDROLYZATION, the DSC curves of PCB-PTHFUs are shown in **Figures 2b and 2c.** The glass transition temperatures of PCB-PTHFU-0, PCB-PTHFU-25, PCB-PTHFU-50, PCB-PTHFU-75, and PCB-PTHFU-100 were -73.4 ℃, - 67.6 ℃, -57.3 ℃, -44.5 ℃, and -8.0 ℃, respectively. The glass transition temperature primarily depends on the chain stiffness of the PCB-PTHFU. PTHF1000 is a long soft segment in PCB-PTHFUs, which increases chain mobility and softness. In comparison, the DEAEA segment is relatively short and stiff. Consequently, the glass transition temperature increases with increasing DEAEA content. The DSC curves of PCB-PTHFUs after hydrolyzation (**Figure S3a and 3b**) are similar to those before hydrolyzation. The glass transition temperature (T_g), crystallization temperature (T_c), and melting temperature (T_m) of hydrolyzed and unhydrolyzed PCB-PTHFUs are summarized in **Table 1**. There is no significant difference in the T_g, T_c, and T_m values before and after hydrolyzation. As hydrolyzation removes only the end ethanol on the DEAEA side chain, the chain stiffness, regularity, symmetry, and the ability to form hydrogen bonding show slight variation; thus, the T_g, T_c, and T_m values remain unchanged.

The T_c of unhydrolyzed PCB-PTHFU-0 and PCB-PTHFU-25 are 8.7 ℃ and -10.9 ℃, respectively, and their T_m is 40.5 ℃ and 28.9 ℃, respectively. For both hydrolyzed and unhydrolyzed samples, PCB-PTHFU-0 crystallized during the cooling process. In contrast, PCB-PTHFU-25 did not crystalize during cooling but crystalize during heating. The well-known fact can explain this difference that cold crystallization is more likely to occur than melt crystallization because nucleation is dampened at higher temperatures.[51] The different behaviors observed for the melt crystallization in PCB-PTHFU-0 and PCB-PTHFU-25 indicate that nucleation is less likely to occur in PCB-PTHFU-25. PCB-PTHFU-50, PCB-PTHFU-75, and PCB-PTHFU-100 show typical DSC curves of amorphous polymers, with no crystallization temperatures or melting temperatures. The above comparison shows that the crystallization capacity decreases with increasing DEAEA content because the DEAEA segment has a lower regularity, symmetry, and softness than the PTHF segment.

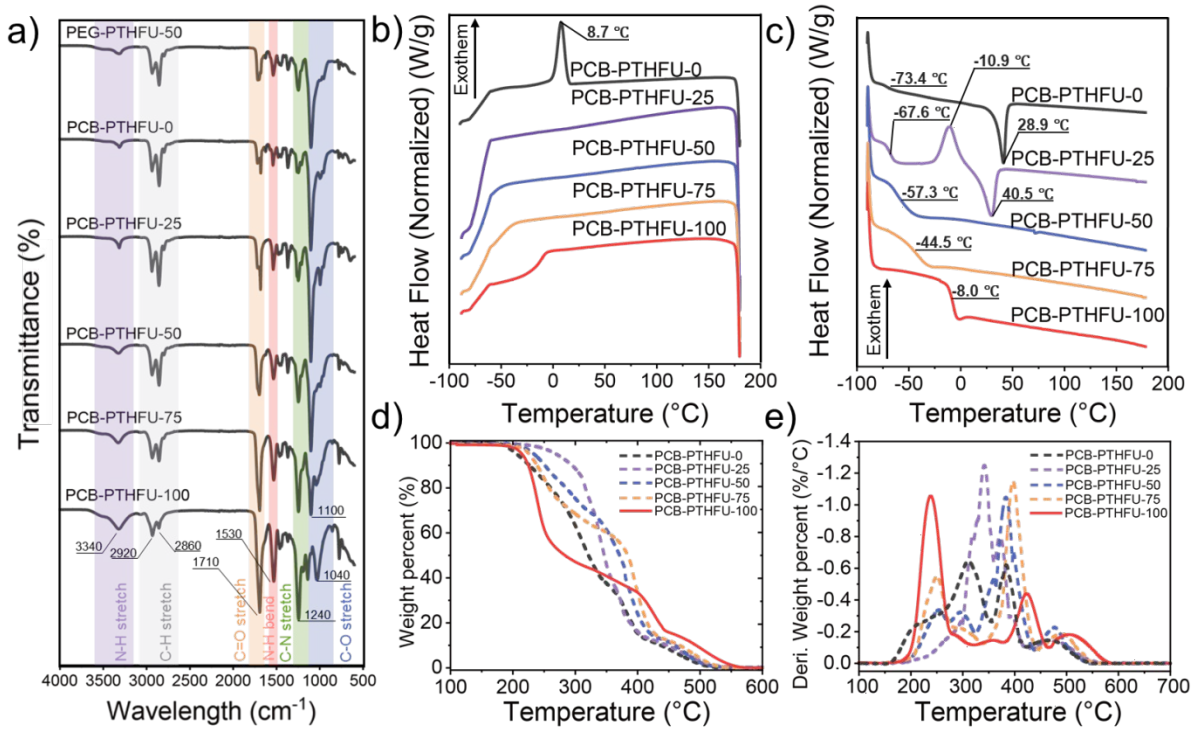

Figure 2. a) FT-IR spectra of PEG-PTHFU-50 and unhydrolyzed PCB-PTHFUs. The absorbance indicates the depletion of reactants and the formation of PCB-PTHFUs with the targeted ratio of DEAEA and PTHF1000. DSC profile of the b) cooling and c) heating curves of unhydrolyzed PCB-PTHFUs. The crystallization behavior of PCB-PTHFUs is revealed. d) TGA and e)

Derivative thermogravimetry (DTG) of unhydrolyzed PCB-PTHFUs. PCB-PTHFUs show an overall high thermal stability.

Table 1. T_g, T_c, and T_m of unhydrolyzed and hydrolyzed PCB-PTHFUs.

	Unhydrolyzed			Hydrolyzed		
	Tg (℃)	Tc (℃)	Tm (℃)	Tg (℃)	Tc (℃)	Tm (℃)
PCB-PTHFU-0	-73.4	8.7	40.5	-70.7	6.6	41.7
PCB-PTHFU-25	-67.6	-10.9	28.9	-68.9	-11.8	29.9
PCB-PTHFU-50	-57.3	-	-	-57.9	-	-
PCB-PTHFU-75	-44.5	-	-	-45.7	-	-
PCB-PTHFU-100	-8.0	-	-	-1.3	-	-

3.4 Rheological testing

The evolution of the storage modulus (G') and loss modulus (G") during heating was studied to evaluate the viscoelastic properties of the PCB-PTHFUs. PCB-PTHFU-0 and PCB-PTHFU-25 show corresponding to a semicrystalline thermoplastic polymer. As shown in **Figures 3a and 3b**, G' was greater than G" at low temperature, at which the polymer is solid and in a rubbery state. As the temperature increases above the melting temperature of PCB-PTHFU-0 (40.5 ℃) and PCB-PTHFU-25 (28.9 ℃), G' and G" undergo a dramatic reduction. After a crossover of G' and G", the polymer became a viscoelastic fluid. The results of a temperature sweep test above 60 ℃, indicating the rheological properties of PCB-PTHFU-0 and PCB-PTHFU-25, are shown in **Figure S4**. PCB-PTHFU-50 and PCB-PTHFU-75 exhibit behavior corresponding to an amorphous thermoplastic polymer. As shown in **Figures 3c and 3d,** the polymers are in a rubbery state at low temperatures, where G' is higher than G". As the temperature increases, both G' and G" gradually decrease. However, G' drops faster than G". When the temperature exceeds 89.6 ℃ for PCB-PTHFU-50 and 142.6 ℃ for PCB-PTHFU-75, the polymer becomes viscoelastic fluid. A temperature sweep test below 60 ℃ for PCB-PTHFU-50 and PCB-PTHFU-75 is shown in **Figure S4**. A frequency rheological study was conducted at 37 ℃ to confirm the behavior of the PCB-PTHFUs at the human body temperature. Except for PCB-PTHFU-25, whose melting temperature was below 37 ℃, all PCB-PTHFUs show G' value higher than G" within the tested frequency range (**Figure S5**). The rheological study of PCB-PTHFU-50 and PCB-PTHFU-75 justifies their application in the fabrication of biomedical devices. Under human body temperature (< 37 ℃),

both polymers are in a rubbery state as a highly elastic stable solid. At higher temperatures that are still below the decomposition temperature, the polymers are a viscoelastic fluid; thus, multiple types of devices can be fabricated by extrusion molding or injection molding.

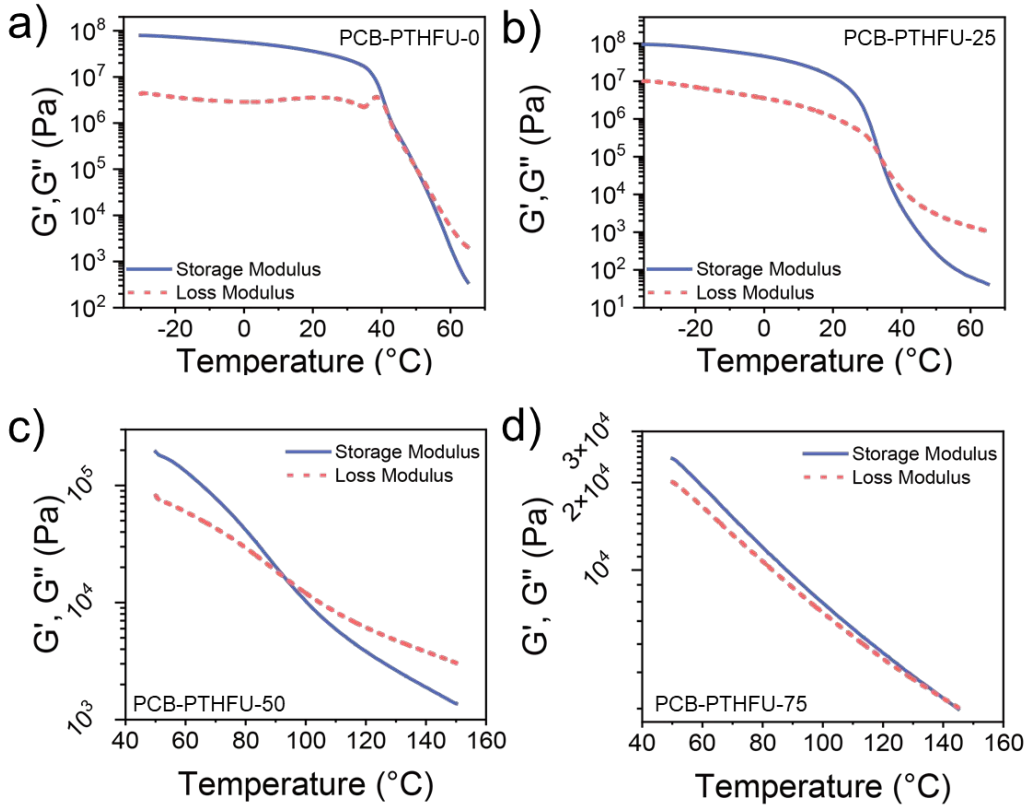

Figure 3. Temperature sweep rheological studies (-35 ℃ to 60 ℃) of a) PCB-PTHFU-0 and b) PCB-PTHFU-25. Temperature sweep rheological studies (60 ℃ to 150 ℃) of c) PCB-PTHFU-50 and d) PCB-PTHFU-75. The polymer becomes viscoelastic fluid at 40.5 ℃, 28.9 ℃, 89.6 ℃, and142.6 ℃ for PCB-PTHFU-0, PCB-PTHFU-25, PCB-PTHFU-50, and PCB-PTHFU-75, respectively.

3.5 Swelling and mechanical properties

The swelling ratios of PCB-PTHFUs vary with the ratio of DEAEA to PTHF. The water uptake of a material depends on its hydrophilicity, intermolecular interaction, and crosslinking density, including its chemical and physical crosslinking. Higher hydrophilicity, weaker intermolecular interactions, and lower crosslinking density result in higher water absorption. Thus, the swelling ratio of the PCB-PTHFUs rises as the ratio of hydrophilic DEAEA increases and the ratio of hydrophobic PTHF decreases, as shown in **Table 2**. PCB-PTHFU-0, PCB-PTHFU-25, PCB-

PTHFU-50, PCB-PTHFU-75, and PCB-PTHFU-100 exhibit swelling ratios of 4.7%, 4.8%, 8.5%, 14.2%, and 20.6%, respectively. Compared with the PCB-PTHFUs, PEG-PTHFU-50 shows a much higher swelling ratio of 23.6%. Although the CB in DEAEA strongly binds water via ionic solvation, the urethane bond density of one DEAEA/HDI repeating unit is much higher than that of PEG/HDI due to the lower molecular weight of DEAEA. The higher urethane bond density leads to stronger overall intermolecular interaction via the hydrogen bond. In addition to the influence of hydrophilicity, the physical crosslinking formed by the crystal region limits the water penetration and swelling. As PCB-PTHFU-0 and PCB-PTHFU-25 are semicrystalline polymers, both show a low swelling ratio of 5 %. Although the PCB-PTHFUs have different swelling ratios in water, their dimensions did not change after equilibration in water, most likely because the physical crosslinking via the hydrogen bonds among the urethane groups inhibited any swelling or dimensional changes.[21, 52] The optical clarities of PCB-PTHFUs are different, as shown in Figure 4. All PCB-PTHFUs with various DEAEA ratios show a translucent color under the dry state. After equilibration in water, the transparency of PCB-PTHFUs can change due to the self-segregation of the hydrophobic PTHF domain and the hydrophilic DEAEA domain. As shown in Figure 4, after two-days equilibration in water, PCB-PTHFU-50 and PCB-PTHFU-75 become opaque for their comparable ratio of the two domains. For PCB-PTHFU-25, although the material contains two domains, the transparency only decreased slightly due to the uneven length of the two domains, the lower water swelling, and the chain movement restriction by the crystalline region. In comparison, PCB-PTHFU-0 and PCB-PTHFU-100 remain transparent as only one domain exists in the material.

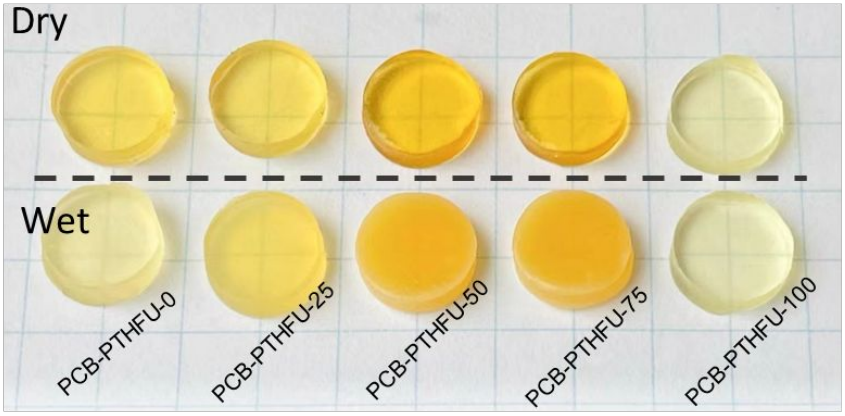

Figure 4. Digital image of PCB-PTHFUs under dry state and after equilibration in water for 2 days. Left to right: PCB-PTHFU-0, PCB-PTHFU-25, PCB-PTHFU-50, PCB-PTHFU-75, and PCB-PTHFU-100.

Compression and tensile tests were performed to evaluate the mechanical properties of the PCB-PTHFUs. None of the unhydrolyzed dry PCB-PTHFUs failed under a maximum 100 MPa stress in the compression study. **Figure 5a** shows partly enlarged strain-stress curves for stresses below 10 MPa. The final strain at maximum stress increases with increasing DEAEA content. PCB-PTHFU-0 and PCB-PTHFU-25 show behaviors corresponding to polymers with a stress plateau at approximately 15 % - 35 % strain and strain hardening at higher strains. In comparison, PCB-PTHFU-50, PCB-PTHFU-75, and PCB-PTHFU-100 behave as amorphous polymers at temperatures above the glass transition temperature, and their stress-strain curves do not exhibit a plateau. This difference is consistent with the DSC results, as PCB-PTHFU-0 and PCB-PTHFU-25 are partly crystallized while the other samples are not. The compression modulus is summarized in **Table 2.** Except for PCB-PTHFU-100, the modulus decreases with increasing the DEAEA composition. The decreasing modulus may be due to a decrease in crystallinity. PCB-PTHFU-0 and PCB-PTHFU-25 exhibit relatively higher modulus values (29.59 MPa and 15.70 MPa) as they are semicrystalline polymers. In comparison, PCB-PTHFU-50 and PCB-PTHFU-75 are amorphous polymers and thus show relatively low modulus values (0.92 MPa and 0.22 MPa). Additionally, the low interfacial strength or stronger phase separation between the soft and hard domains could result in a lower modulus. The chain length difference between the DEAEA and PTHF1000 segments decreases with increasing DEAEA ratio, as PCB-PTHFU-75 possesses the most balanced DEAEA and PTHF100 length ratio. Besides, the decreasing molecular weight of PCB-PTHFUs (Figure S2) with increasing DEAEA segment also contributes to decreasing the modulus. Thus, the lowest modulus is observed for PCB-PTHFU-75. PCB-PTHFU-100, although with the lowest molecular weight among PCB-PTHFUs, shows a higher modulus value (2.74 MPa) than PCB-PTHFU-50 and PCB-PTHFU-75 due to the absence of the PTHF chain, which results in low phase segregation and high hydrogen bonding density.

Compression strain-stress curves of the PCB-PTHFUs after hydrolysis are shown in **Figures 5b and 5c**. PCB-PTHFU-0 show breakage at a strain of 18%, while the remaining PCB-PTHFUs did not show any failure at a maximum stress of 100 MPa after hydrolysis. However, all PCB-PTHFUs show a decrease in compression modulus after hydrolysis. PCB-PTHFU-0, PCB-PTHFU-25,

PCB-PTHFU-50, PCB-PTHFU-75, and PCB-PTHFU-100 exhibit modulus values of 27.67, 15.04, 0.23, 0.06, and 3.09 MPa, respectively. The breakage of PCB-PTHFU-0 and the modulus change can be affected by the swelling of materials and the decrease in hydrogen bonding density. The modulus change after hydrolysis is largely related to the swelling ratio of the PCB-PTHFUs. Except for PCB-PTHFU-100, the decrease in the PCB-PTHFU modulus in water enlarges with increasing DEAEA content. The compression modulus of PCB-PTHFU-0 decreases by 6.4% after hydrolysis, whereas that of PCB-PTHFU-75 decreases by 72.7%. This large difference in the modulus change is due to the larger swelling ratio of PCB-PTHFUs with increasing DEAEA content. PCB-PTHFU-100 shows a relatively small modulus variation after hydrolysis, most likely due to a high level of physical crosslinking by the inter-and intramolecular hydrogen bonding.

The tensile behavior of the PCB-PTHFUs is shown in **Figure 5d**. Except for PCB-PTHFU-100, the breaking stress values decrease and the breaking strain values increase with increasing DEAEA ratio. This trend may be due to a decrease in crystallinity and interfacial strength, as discussed above. PCB-PTHFU-100 shows a relatively high stiffness, possibly due to the high hydrogen-bonding density. The breaking strains are summarized in **Table 2**. Tensile tests of PCB-PTHFUs after hydrolysis were performed and compared with those before hydrolysis, as shown in **Figures 5e** and **5f**. After hydrolysis, the breaking strains of the PCB-PTHFUs decrease by 47%-60% due to the absorption of water and a decrease in hydrogen bonding density. Compression and tensile tests were also performed for PEG-PTHFU-50 as a reference. As shown in **Figure 5** and **Table 2**, PEG-PTHFU-50 exhibits a modulus of 1.11 MPa after water equilibration, which decreased by 84% compared with the dry state due to the high water uptake of PEG-PTHFU-50. In addition, PEG-PTHFU-50 shows a breaking strain of 6.8% for the tensile test in the wet state. These compression and tensile tests demonstrate the soft and brittle mechanical properties of PEG-PTHFU-50, especially after hydrolysis. Although PEG-PTHFU-50 is confirmed to exhibit antifouling properties to some extent, as discussed in a later section, the bio-application of these material may be limited by its mechanical strength.

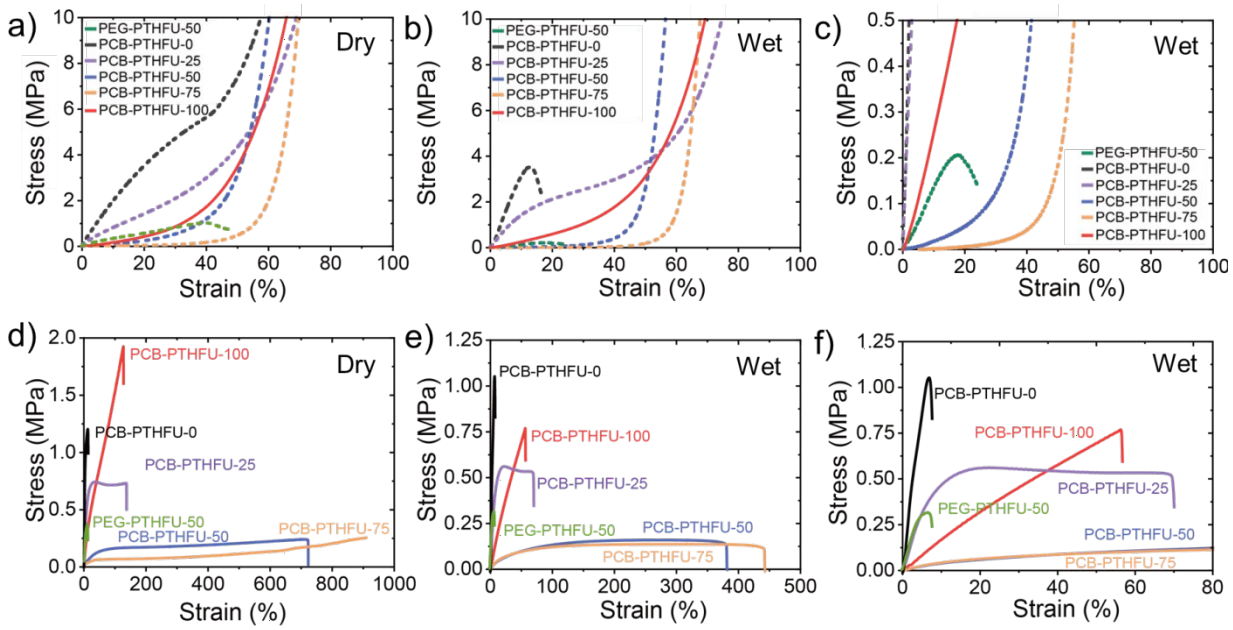

Figure 5. Compression strain-stress curves of a) unhydrolyzed PCB-PTHFUs in the dry state and b) hydrolyzed PCB-PTHFUs in the wet state. c) Partially enlarged view of Figure 3b. PCB-PTHFU-0 show breakage at a strain of 18%, while the remaining PCB-PTHFUs did not show any failure at a maximum stress of 100 MPa after hydrolysis. Except for PCB-PTHFU-100, the decrease in the PCB-PTHFU modulus in water enlarges with increasing DEAEA content. Tensile strain-stress curves of d) unhydrolyzed PCB-PTHFUs in the dry state and e) hydrolyzed PCB-PTHFUs in the wet state. f) Partially enlarged view of Figure 3e. The breaking stress values decrease and the breaking strain values increase with increasing DEAEA ratio expect for PCB-PTHFU-100. After hydrolysis, the breaking strains of the PCB-PTHFUs decrease by 47%-60%.

Table 2. Young's modulus from compression test, breaking strain in the tensile test, and swelling ratio of PCB-PTHFUs.

	Young's Modulus from compression test (MPa)		Breaking strain from tensile test (%)		Swelling ratio (%)
	Dry	Wet	Dry	Wet	
PEG-PTHFU-50	6.94	1.11	10.7	6.8	23.6
PCB-PTHFU-0	29.59	27.67	13.2	6.9	4.7
PCB-PTHFU-25	15.70	15.04	172.8	68.8	4.8
PCB-PTHFU-50	0.92	0.23	722.5	379.5	8.5

PCB-PTHFU-75	0.22	0.06	909.4	442.7	14.2
PCB-PTHFU-100	2.74	3.09	127.3	57.7	20.6

3.6 Protein adsorption

Protein adsorption on a material surface results in a conditional layer that initiates further attachment of organisms, which causes blood coagulation, foreign body reactions, biofilms, and infection.[3] To address these biofouling issues, it was hypothesized that zwitterionic CB moieties may reduce nonspecific protein adsorption. Fibrinogen (Fg) has been widely used as a standard in vitro screening tool to assess protein adsorption levels, as it can strongly adsorb onto a variety of surfaces.[53] In this work, a fluorescence method was used to characterize the fibrinogen adsorption on PCB-PTHFU surfaces. A PEG-based material (PEG-PTHFU-50) and commercially available medical grade polyurethane (API-PU) were used as references. The API-PU is an aromatic polyether thermoplastic polyurethane with good resistance to microbial. It was reported that the API-PU shows a 98.7% reduction of E.coli growth compared with polyethylene.[54] The antimicrobial performance of API-PU makes it a good reference in studying the anti-fouling property of PCB-PTHFUs. Thus, the protein adsorption levels of the materials tested in this study was expressed as a percentage based on the API-PU level (100%). As shown in **Figure 6a**, without hydrolysis, PCB-PTHFU-0 exhibits the highest protein adsorption level at 270% of API-PU due to the intrinsic hydrophobicity of PTHF1000. In contrast, PCB-PTHFU-25, PCB-PTHFU-50, PCB-PTHFU-75, and PCB-PTHFU-100, which contain hydrophilic DEAEA segments, show less protein adsorption than PCB-PTHFU-0 (70% - 200% relative to API-PU). Overall, without hydrolysis, the PCB-PTHFUs show similar protein adsorption compared with API-PU. However, after 120 min of rapid hydrolysis of DEAEA in a PBS buffer at pH 8.5, the protein adsorption of the PCB-PTHFUs decreases significantly. The Fg adsorption on PCB-PTHFU-50, PCB-PTHFU-75, and PCB-PTHFU-100 is less than 10% of that on API-PU, indicating that protein adsorption on the material surface is effectively controlled. The Fg adsorption on PCB-PTHFU-25 decreases from 193% before hydrolysis to 24.3%. Although PCB-PTHFU-25 contains the DEAEA zwitterionic precursor group, the concentration of DEAEA is only 25%. Thus, it is possible that there are not enough CB groups on the surface of PCB-PTHFU-25, which can provide sufficient resistance to protein adsorption. In the case of PCB-PTHFU-0, there is no hydrolysable zwitterionic precursor. However, PCB-PTHFU-0 also shows a decrease in protein adsorption after

120 min of equilibration in a pH-8.5 PBS buffer (98% relative to API-PU). The decreased protein adsorption on PCB-PTHFU-0 may be attributed to the swelling of the material and wetting of the surface during equilibration. In water, a longer time is required for the completion of self-catalyzed hydrolysis because the hydroxide concentration that drives the process can be reduced by the hydrolysis of CB. After 48 h of equilibration in water, the PCB-PTHFUs switch to the zwitterionic state with an apparent decrease in fibrinogen adsorption. The Fg adsorption on PCB-PTHFU-50, PCB-PTHFU-75, and PCB-PTHFU-100 is less than 10% of that for API-PU (**Figure 6b**). The results of the fluorescence study indicate that PCB-PTHFU-50, PCB-PTHFU-75, and PCB-PTHFU-100 are effective at resisting nonspecific protein adsorption. The PCB-PTHFUs benefit from the zwitterionic CB groups generated via hydrolysis. He *et al*. demonstrated that zwitterionic materials can form a strong hydration layer that provides an effective barrier to prevent foulants from interacting with the material surfaces, thus leading to a significant decrease in protein adsorption.[32] As PEG-based functionalization has been widely used as a gold standard for improving the antifouling property of materials, we also synthesized PEG-PTHFU-50 as a reference. PEG-PTHFU-50 shows relatively consistent protein adsorption behavior under all conditions, with an average adsorption of 52% compared with API-PU. Although PEG-PTHFU-50 shows less protein adsorption than API-PU, the adsorption level is still higher than that of the hydrolyzed zwitterionic PCB-PTHFUs. The Fg adsorption study further demonstrates that the CB functional group is more efficient than PEG in resisting nonspecific protein adsorption.

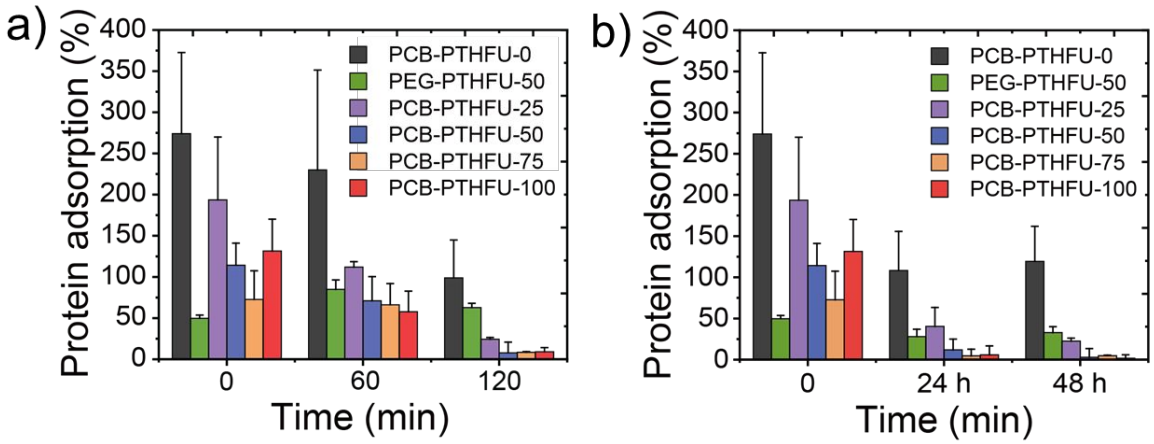

Figure 6. a) Protein adsorption on surfaces of PCB-PTHFUs after incubation in (a) pH-8.5 PBS buffer and (b) water for different lengths of time. Commercially available API-PU and PEG-PTHFU-50 were used as control materials. After 120 min of rapid hydrolysis in a PBS buffer at

pH 8.5 or 48 h of equilibration in water, the Fg adsorption on PCB-PTHFU-50, PCB-PTHFU-75, and PCB-PTHFU-100 is less than 10% of that for API-PU.

3.7 Mammalian cell attachment

Common causes of failure for implanted medical devices include thrombosis and (foreign body response) FBR, which are induced by protein attachment and subsequent adsorption of platelets, fibroblasts, and macrophages. To evaluate the resistance to mammalian cells attachment on PCB-PTHFUs, cell adhesion experiments were performed with NIH-3T3 fibroblast cells. Before exposing the materials to cells, we immersed the PCB-PTHFUs in 100% FBS for 14 days to allow the absorption of serum proteins. As implanted medical devices are continuously exposed to body fluid or blood, our experiment can better mimic the *in vivo* environment. Afterward, PCB-PTHFUs were incubated with NIH-3T3 cells at 37 °C for 24 h and examined by bright-field microscopy. **Figure 7** shows that the cell densities on the API-PU, PCB-PTHFU-0, and PCB-PTHFU-25 surfaces are 9.8×10^4 cells/cm^2, 7.8×10^4 cells/cm^2, and 7.2×10^4 cells/cm^2, respectively. No attached cells were observed on the surfaces of PCB-PTHFU-50, PCB-PTHFU-75, or PCB-PTHFU-100. These test results demonstrate that, even in a complex protein-rich medium, mammalian cell attachments can be effectively prevented by the zwitterionic CB moieties.

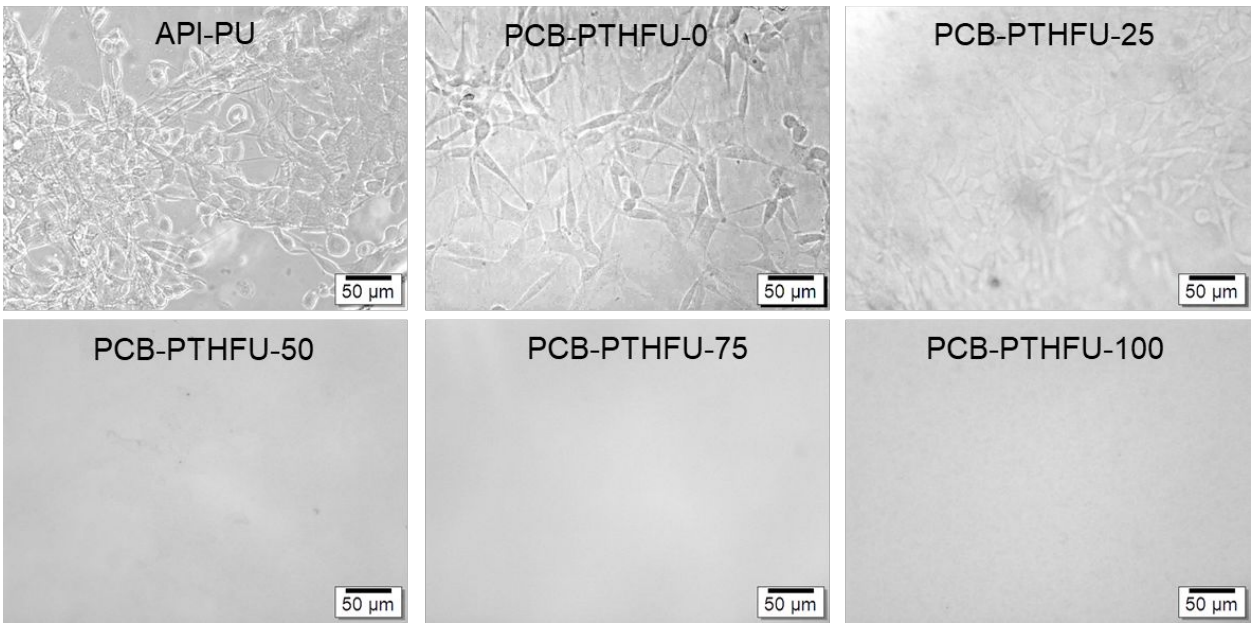

Figure 7. Cell attachment of PCB-PTHFUs after hydrolysis. Commercially available API-PU was used as a control. The scale bar is 50 μm. No attached cells were observed on the surfaces of PCB-PTHFU-50, PCB-PTHFU-75, or PCB-PTHFU-100 after incubation at 37 °C for 24 h.

3.8 Bacterial attachment and biofilm

In addition to thrombosis and FBR, infection and biofilms are another two other significant causes of implant failure. The presence of zwitterionic CB moieties on a material surface has proven to be critical for resisting bacterial attachment and biofilm formation.[21] As a consequence, we expect PCB-PTHFUs to effectively resist the attachment of bacterial cells. Short-term bacterial cell attachment onto the PCB-PTHFUs was evaluated using P. aeruginosa PAO1 bacteria, one of the most common pathogens causing infections associated with catheters and foreign body implants. All PCB-PTHFUs were repeatedly exposed to a high-concentration bacterial suspension and then dried. The bacterial attachment after each cycle was evaluated. A large number of bacteria were observed in the first exposure for API-PU, PCB-PTHFU-0, and PCB-PTHFU-25. The bacterial density on the material increases with repetitive exposure to the bacterial suspension. For API-PU, the bacterial density increases to 9.0×10^6 cells/cm^2 after three cycles (**Figure 8**) and remains at a constant level throughout the remainder of the tests. Meanwhile, PEG-PTHFU-50 and PCB-PTHFU-50 show lower bacterial attachment. However, after seven cycles, the cell density on PEG-PTHFU-50 increased to 3.7×10^6 cells/cm^2. PCB-PTHFU-75 shows an attachment below 1.1×10^6 cells/cm^2 for *P. aeruginosa* PAO1 after seven cycles, representing an average decrease of 86.6% compared with API-PU. PCB-PTHFU-100 shows minimal bacterial attachment, with almost no cells observed. The ionic solvation between the zwitterionic moiety and water molecules can form a hydration layer that strongly resists to bacterial attachment on PCB-PTHFUs, especially for materials with relatively high-density zwitterionic components, such as PCB-PTHFU-75 and PCB-PTHFU-100. Repeated exposure for one week was applied to mimic the use of coatings and devices, such as the reuse of intermittent urine catheters, in real life. A reusable catheter is favorable due to its low cost with less waste.[55] However, the incidence of urethral trauma and urinary tract infection has been reported to reach 70%–80% for reused catheters.[56] The experiment in our studies considers a more challenging situation than the actual application of reusable catheters, as the samples were not sterilized between cycles. Additionally, a higher cell concentration was used in the bacterial suspension (5×10^8 cells/mL) instead of the concentration observed during short-term urine contact ($<10^5$ cells/mL).[57] The results of our bacterial attachment test demonstrate the potential application of PCB-PTHFUs for the reusable implanted devices.

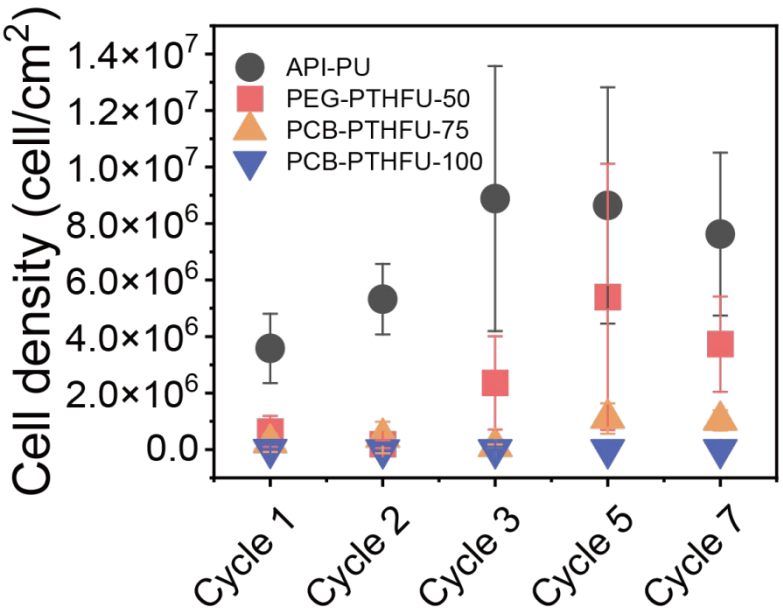

Figure 8. Cell density on PCB-PTHFUs during a repeatedly exposed to a high-concentration bacterial suspension and then dried. API-PU shows a large number of bacteria in the first exposure. In comparison, PEG-PTHFU-50 show lower bacterial attachment, PCB-PTHFU-75 shows an average decrease of 86.6% compared with API-PU, and PCB-PTHFU-100 shows almost no cells observed.

The long-term biofilm formation of *P. aeruginosa* PAO1, which is a critical challenge for indwelling urinary catheters, was also studied on PCB-PTHFU surfaces. Previous studies by Wang *et al.* demonstrated that polymers with zwitterionic CB moieties can completely prevent biofilm formation for up to six months.[21] However, no highly elastic thermoplastic polymer material has shown critical long-term resistance to biofilm formation in a complex system. In this study, biofilm formation was evaluated under a challenging static environment with a protein-rich complex growth medium that helps bacterial cells attach to the surface and provides nutrients for the rapid growth of biofilms. As shown in **Figure 9**, biofilms grew rapidly on the surface of API-PI, PCB-PTHFU-0, and PCB-PTHFU-25, with over 75% of the material surface covered by biofilm after one day of incubation. In comparison, PEG-based PEG-PTHFU-50 shows less biofilm formation with a minimal level of biofilm found on the first day. However, after three days of incubation, the PEG-PTHFU-50 surface was almost entirely covered by *P. aeruginosa*, as observed for API-PU. In contrast, PCB-PTHFU-50 shows three-day delay in biofilm growth on the surface. After five days in *P. aeruginosa* PAO1 culture, PCB-PTHFU-50 shows a biofilm surface coverage of 8.95%,

and the coverage increased to 48.7% after one week. Because PCB-PTHFU-50 possesses a higher CB density than PCB-PTHFU-25, it is more resistant to biofilm formation than PCB-PTHFU-25. However, the density of zwitterionic CB moieties could still be insufficient to provide a longer-term biofilm-free surface. In comparison, almost no *P. aeruginosa* PAO1 bacterial cells were observed on the PCB-PTHFU-75 and PCB-PTHFU-100 surfaces, even after three weeks.

Biofilm adhesion on unhydrolyzed dry PCB-PTHFUs was also evaluated with dry PEG-PTHFU-50 and API-PU. Of note, dry material samples were placed directly in the protein-rich medium for biofilm growth, without pre-hydrolysis or buffer equilibration. The hydrolysis of PCB-PTHFUs and the generation of antifouling zwitterionic CB groups compete with the biofilm growth. As shown in **Figure 10**, the biofilm grew rapidly on API-PI, PEG-PTHFU-50, PCB-PTHFU-0, and PCB-PTHFU-25, with over 80% of the material surface covered by biofilm after one day of incubation and almost complete coverage after three days. Dry PEG-PTHFU-50 does not show the same mitigated biofilm formation that occurs when it is equilibrated with water. The pre-equilibrated PEG-PTHFU-50 may experience micro-phase segregation in water and expose more hydrophilic PEG segments being exposed on the material surface, thus showing better biofilm resistance than dry PEG-PTHFU-50. PCB-PTHFU-50 shows less biofilm growth on the surface, with 38.67% biofilm surface coverage on the first day and 58.97% coverage on the second day. After three days of incubation, the surface of PCB-PTHFU-50 was almost completely covered by biofilm. PCB-PTHFU-75 and PCB-PTHFU-100 show biofilm growth on the first day with 45.20% and 8.27% biofilm coverage on the surface, respectively. However, as hydrolysis of the material occurred in the broth medium, PCB-PTHFU-75 and PCB-PTHFU-100 show a release of surface biofilm starting on the second day and found biofilm-free on the third and fourth day, respectively. After three weeks, PCB-PTHFU-75 and PCB-PTHFU-100 exhibit no *P. aeruginosa* PAO1 cells. Our results show that zwitterionic PCB-PTHFUs surfaces possess an excellent ability to resist biofilm formation. The rapid self-catalyzed hydrolysis of DEAEA can provide a high resistance to biofilm formation and can release biofilms, even without pre-hydrolyzation.

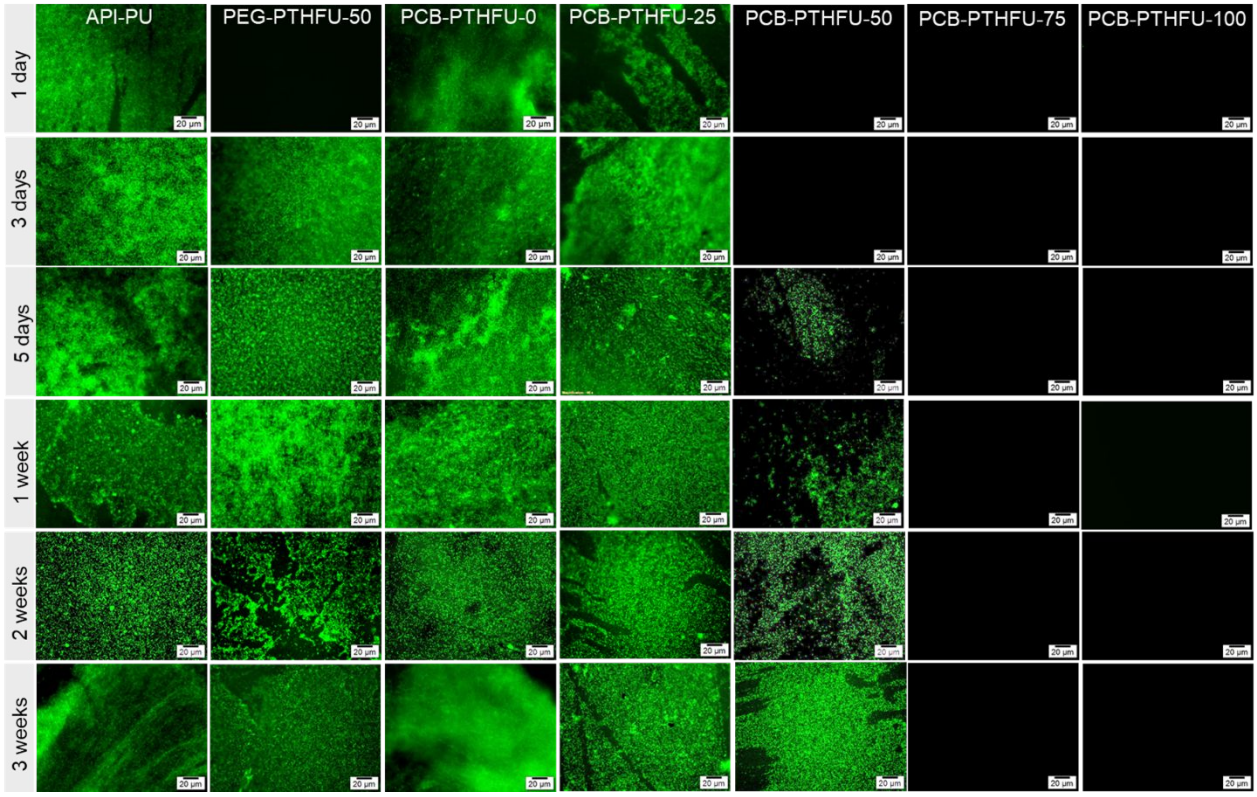

Figure 9. Fluorescence images of the biofilm formation of *P. aeruginosa* PAO1 on hydrolyzed PCB-PTHFUs. Commercially available API-PU and PEG-PTHFU50 were used as control materials. The scale bar is 20 μm. Almost no P. aeruginosa PAO1 bacterial cells were observed on the PCB-PTHFU-75 and PCB-PTHFU-100 surfaces after three weeks.

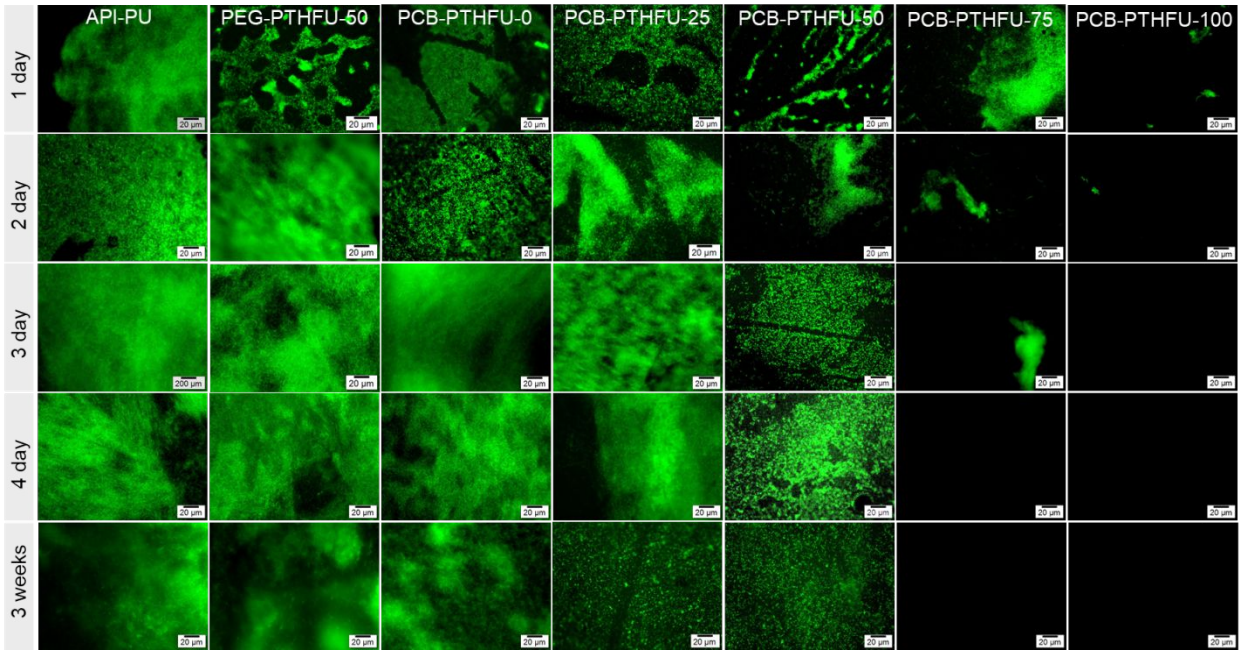

Figure 10. Fluorescence images of the biofilm formation of *P. aeruginosa* PAO1 on unhydrolyzed PCB-PTHFUs. Commercially available API-PU and PEG-PTHFU50 were used as control materials. The scale bar is 20 μm. As hydrolysis of the material occurred in the broth medium, PCB-PTHFU-75 and PCB-PTHFU-100 show a release of surface biofilm starting on the second day and found biofilm-free on the third and fourth day.

4. Conclusions

This study demonstrates a facile strategy for synthesizing a thermoplastic polyurethane with enhanced elasticity and superior antifouling properties. A series of zwitterionic PCB-PTHFUs was synthesized with CB and PTHF1000 as part of the PU backbone, where the CB content in the polymer was optimized by altering the molar ratio of DEAEA and PTHF1000. PCB-PTHFUs with high CB content, such as PCB-PTHFU-75 and PCB-PTHFU-100, displayed the ability to resist cell attachment for 24 h and to prevent biofilm formation for three weeks. Additionally, the PTHF1000 segment was found to enhance the elasticity of the PCB-PTHFUs and provided a 400% breaking strain compared with PCB-PTHFU-75. This study provides fundamental information regarding the structure–function relationships of zwitterionic polymers. This highly elastic thermoplastic PCB-PTHFU platform with critical antifouling properties can be applied for a wide range of applications, including implanted medical devices. The PCB-PTHFUs exhibited a breaking strain of more than 400%, high resistance to fibroblast cells for 24 h, and the ability to prevent biofilm formation for up to three weeks. This study lays a foundation for fundamentally elucidating the structure–function relationships of zwitterionic polymers.

Acknowledgment

This work was supported by the US National Science Foundation (DMR-1454837 and 1741935).

1. Z. Khatoon, C. D. McTiernan, E. J. Suuronen, T.-F. Mah and E. I. Alarcon, *Heliyon*, 2018, **4**, e01067.
2. B. W. Trautner and R. O. Darouiche, *Archives of Internal Medicine*, 2004, **164**, 842.
3. L. E. Nicolle, *Antimicrobial Resistance and Infection Control*, 2014, **3**, 23.
4. N. Maccallum, C. Howell, P. Kim, D. Sun, R. Friedlander, J. Ranisau, O. Ahanotu, J. J. Lin, A. Vena, B. Hatton, T.-S. Wong and J. Aizenberg, *ACS Biomaterials Science & Engineering*, 2015, **1**, 43-51.
5. W. Khan, E. Muntimadugu, M. Jaffe and A. J. Domb, Springer US, 2014, DOI: 10.1007/978-1-4614-9434-8_2, pp. 33-59.
6. R. E. W. Hancock and D. P. Speert, *Drug Resistance Updates*, 2000, **3**, 247-255.
7. S. P. Nikam, P. Chen, K. Nettleton, Y.-H. Hsu and M. L. Becker, *Biomacromolecules*, 2020, **21**, 2714-2725.
8. P. Krol, *Progress in Materials Science*, 2007, **52**, 915-1015.
9. J. Joseph, R. M. Patel, A. Wenham and J. R. Smith, *Transactions of the IMF*, 2018, **96**, 121-129.
10. Y. Hong, in *Advances in polyurethane biomaterials*, Elsevier, 2016, pp. 543-559.
11. J. W. Costerton, P. S. Stewart and E. P. Greenberg, *Science*, 1999, **284**, 1318-1322.
12. P. Liu, T. Huang, P. Liu, S. Shi, Q. Chen, L. Li and J. Shen, *J Colloid Interface Sci*, 2016, **480**, 91-101.
13. K. D. Park, Y. S. Kim, D. K. Han, Y. H. Kim, E. H. B. Lee, H. Suh and K. S. Choi, *Biomaterials*, 1998, **19**, 851-859.
14. H. Shi, H. Liu, S. Luan, D. Shi, S. Yan, C. Liu, R. K. Y. Li and J. Yin, *Composites Science and Technology*, 2016, **127**, 28-35.
15. K. Li, Y. Qi, Y. Zhou, X. Sun and Z. Zhang, *Polymers*, 2021, **13**, 573.
16. Z. Xie, N. V. Aphale, T. D. Kadapure, A. S. Wadajkar, S. Orr, D. Gyawali, G. Qian, K. T. Nguyen and J. Yang, *Journal of Biomedical Materials Research Part A*, 2015, **103**, 3907-3918.
17. J. Ladd, Z. Zhang, S. Chen, J. C. Hower and S. Jiang, *Biomacromolecules*, 2008, **9**, 1357-1361.
18. H. Wang, Y. Hu, D. Lynch, M. Young, S. Li, H. Cong, F. J. Xu and G. Cheng, *ACS Appl. Mater. Interfaces*, 2018, **10**, 37609-37617.
19. M. D. Swartzlander, C. A. Barnes, A. K. Blakney, J. L. Kaar, T. R. Kyriakides and S. J. Bryant, *Biomaterials*, 2015, **41**, 26-36.
20. X. Wang, T. Ishida and H. Kiwada, *Journal of Controlled Release*, 2007, **119**, 236-244.
21. H. Wang, D. E. Christiansen, S. Mehraeen and G. Cheng, *Chemical Science*, 2020, **11**, 4709-4721.
22. B. Cao, C. Lee, Z. Zeng, F. Cheng, F. Xu, H. Cong and G. Cheng, *Chem. Sci.*, 2016, **7**, 1976-1981.
23. B. Cao, Q. Tang and G. Cheng, *Journal of Biomaterials Science, Polymer Edition*, 2014, **25**, 1502-1513.
24. B. Cao, L. Li, Q. Tang and G. Cheng, *Biomaterials*, 2013, **34**, 7592-7600.
25. B. Cao, Q. Tang, L. Li, J. Humble, H. Wu, L. Liu and G. Cheng, *Advanced Healthcare Materials*, 2013, **2**, 1096-1102.
26. B. Cao, Q. Tang, L. Li, C. J. Lee, H. Wang, Y. Zhang, H. Castaneda and G. Cheng, *Chem. Sci.*, 2015, **6**, 782-788.
27. A. n. A. Beltrán-Osuna, B. Cao, G. Cheng, S. C. Jana, M. P. Espe and B. Lama, *Langmuir*, 2012, **28**, 9700-9706.
28. A. Venault and Y. Chang, *Langmuir*, 2019, **35**, 1714-1726.
29. S. Kim, S.-H. Ye, A. Adamo, R. A. Orizondo, J. Jo, S. K. Cho and W. R. Wagner, *Journal of Materials Chemistry B*, 2020, **8**, 8305-8314.
30. D. Dong, C. Tsao, H.-C. Hung, F. Yao, C. Tang, L. Niu, J. Ma, J. MacArthur, A. Sinclair and K. Wu, *Science advances*, 2021, **7**, eabc5442.
31. X. Li, C. Tang, D. Liu, Z. Yuan, H. C. Hung, S. Luozhong, W. Gu, K. Wu and S. Jiang, *Advanced Materials*, 2021, **33**, 2102479.

32. M. He, K. Gao, L. Zhou, Z. Jiao, M. Wu, J. Cao, X. You, Z. Cai, Y. Su and Z. Jiang, *Acta Biomaterialia*, 2016, **40**, 142-152.
33. J. B. Schlenoff, *Langmuir*, 2014, **30**, 9625-9636.
34. W. Ma, T. Chen, S. Nanni, L. Yang, Z. Ye and M. S. Rahaman, *Langmuir*, 2019, **35**, 1513-1525.
35. H. Chen, M. Zhang, J. Yang, C. Zhao, R. Hu, Q. Chen, Y. Chang and J. Zheng, *Langmuir*, 2014, **30**, 10398-10409.
36. S. C. Lange, E. Van Andel, M. M. J. Smulders and H. Zuilhof, *Langmuir*, 2016, **32**, 10199-10205.
37. L. Carr, G. Cheng, H. Xue and S. Jiang, *Langmuir*, 2010, **26**, 14793-14798.
38. Y. He, H.-K. Tsao and S. Jiang, *The Journal of Physical Chemistry B*, 2012, **116**, 5766-5770.
39. P. N. Coneski and J. H. Wynne, *ACS Appl Mater Interfaces*, 2012, **4**, 4465-4469.
40. S. Chen, F. Mo, Y. Yang, F. J. Stadler, S. Chen, H. Yang and Z. Ge, *Journal of Materials Chemistry A*, 2015, **3**, 2924-2933.
41. S. Liu, J. Tang, F. Ji, W. Lin and S. Chen, *Gels*, 2022, **8**, 46.
42. Q. Chen, S. Liang and G. A. Thouas, *Progress in Polymer Science*, 2013, **38**, 584-671.
43. A. J. T. Teo, A. Mishra, I. Park, Y.-J. Kim, W.-T. Park and Y.-J. Yoon, *ACS Biomaterials Science & Engineering*, 2016, **2**, 454-472.
44. Z. K. Zander and M. L. Becker, *ACS Macro Letters*, 2018, **7**, 16-25.
45. B. Cao, L. Li, H. Wu, Q. Tang, B. Sun, H. Dong, J. Zhe and G. Cheng, *Chem Commun (Camb)*, 2014, **50**, 3234-3237.
46. C. Prisacariu, *Polyurethane elastomers: from morphology to mechanical aspects*, Springer Science & Business Media, 2011.
47. P. Kordomenos and J. Kresta, *Macromolecules*, 1981, **14**, 1434-1437.
48. Z. S. Petrović, Z. Zavargo, J. H. Flyn and W. J. Macknight, *Journal of Applied Polymer Science*, 1994, **51**, 1087-1095.
49. M. Berta, C. Lindsay, G. Pans and G. Camino, *Polym. Degrad. Stab.*, 2006, **91**, 1179-1191.
50. D. K. Chattopadhyay and D. C. Webster, *Progress in Polymer Science*, 2009, **34**, 1068-1133.
51. P. Badrinarayanan, K. B. Dowdy and M. R. Kessler, *Polymer*, 2010, **51**, 4611-4618.
52. X. Peng, H. Liu, Q. Yin, J. Wu, P. Chen, G. Zhang, G. Liu, C. Wu and Y. Xie, *Nature Communications*, 2016, **7**, 11782.
53. T. A. Horbett, *Journal of Biomedical Materials Research Part A*, 2018, **106**, 2777-2788.
54. API, Antimicrobial TPU Film, https://www.americanpolyfilm.com/antimicrobial-tpu-film, (accessed 3/22, 2022).
55. M. Avery, J. Prieto, I. Okamoto, S. Cullen, B. Clancy, K. N. Moore, M. Macaulay and M. Fader, *BMJ Open*, 2018, **8**, e021554.
56. M. Å. Håkansson, *Spinal Cord*, 2014, **52**, 511-516.
57. B. W. Trautner and R. O. Darouiche, *American Journal of Infection Control*, 2004, **32**, 177-183.